

PHYSICAL REVIEW C

NUCLEAR PHYSICS

THIRD SERIES, VOLUME 38, NUMBER 2

AUGUST 1988

Electron scattering form factors of stretched transitions using Woods-Saxon wave functions

B. L. Clausen* and R. J. Peterson

Nuclear Physics Laboratory, University of Colorado, Boulder, Colorado 80309

R. A. Lindgren

Institute of Nuclear and Particle Physics and Physics Department, University of Virginia, Charlottesville, Virginia 22904

(Received 15 September 1987; revised manuscript received 29 April 1988)

Electron scattering form factors for stretched transitions are computed using radial wave functions from realistic nuclear potentials, including the unbound nature of final states above particle decay thresholds. The calculated form factors are compared to data for 4^- states in ^{12}C , ^{14}C , and ^{16}O , 6^- states in ^{24}Mg , ^{26}Mg , and ^{28}Si , 8^- states in ^{48}Ca , ^{54}Fe , ^{58}Ni , and ^{60}Ni , the 10^- state in ^{90}Zr , and the 14^- state in ^{208}Pb . We assess the fraction of the single-particle sum rule strengths using these realistic nuclear potentials in place of the standard results using harmonic oscillator wave functions. Appreciably greater fractions are obtained for low mass nuclei in the present work, totaling 105% of the sum strength for ^{12}C and 81% for ^{16}O . Much less damping of the magnetic strength is thus experimentally observed than is the case when oscillator wave functions are used for comparison. The results of including meson exchange currents in the analysis are also discussed.

I. INTRODUCTION

The systematic failure of theory to account for the observed quenching of the transition strength for magnetic nuclear excitations is an important unresolved problem in nuclear physics.¹ The loss of magnetic strength at low multipoles such as observed for 1^+ states in Gamow-Teller (p,n) reactions² and in electron scattering^{3,4} has been partially accounted for by including core polarization, ground-state correlations, and mixing with the delta-particle nucleon-hole states in the nucleus. Recently,⁵⁻⁷ discrepancies between theory and experiment for magnetic excitations were related to the role of the occupation number distributions in the nuclear ground states. For high-spin magnetic multipole excitations, it was expected that fewer difficulties would stand in the way of more completely understanding the magnetic strength to stretched excitations because mixing with the subnucleon degrees of freedom is negligible and nuclear configuration mixing may be minimal due to the uniqueness of the maximally stretched particle-hole configuration.⁸ However, systematic quenching of the transition strength to stretched states is observed. Systematic shell-model studies, which include configuration mixing in the ground and excited states, predict too much cross section by at least a factor of 2 for many of the observed transitions.⁹ Including meson exchange currents in the analysis of the elec-

tron scattering data to stretched states results in yet further disagreement between experiment and theory.¹⁰

The principal means of investigating high-spin particle-hole states has been by inelastic electron scattering. The fraction of the single-particle strength exhausted by the data has been evaluated most commonly by comparing the experimental transverse (magnetic) form factor to the form factor calculated in the extreme single-particle shell model. For simplicity, and to provide systematics over a wide range of nuclei, strengths have been previously extracted using harmonic oscillator radial wave functions.^{11,12} For example, see the ($f_{7/2}d_{5/2}^{-1}$) 6^- states in the sd shell¹² and the ($g_{9/2}f_{7/2}^{-1}$) 8^- states in the fp shell.¹¹

The states of interest lie at fairly high excitation energies, sometimes above the proton and/or neutron separation energies, and thus the radial wave functions for the final states may extend greatly beyond those computed for a harmonic oscillator (HO). Even the isospin symmetry that is usually assumed in HO calculations is in doubt, since neutron and proton wave functions may differ substantially due to their differing decay probabilities. These effects are accounted for in bound-state Woods-Saxon (WS) well calculations, extended in this work to states unbound to particle decay. Consequently, overlap integrals used in computing the form factors will differ for protons and neutrons, which could significantly

influence the total strength extracted from the data.

In this paper we calculate the neutron and proton transition densities to 52 stretched states in 12 different nuclei using radial wave functions computed for nucleons in a WS potential by the computer code DWUCK4.¹³ For cases where the nucleon is unbound, the excited nucleon is treated as a resonance by a method well-established for single-nucleon stripping reactions.¹⁴ Comparisons are made to results from HO potentials. We also discuss the influence of meson exchange currents¹⁵ (MEC) on the extracted single-particle strength.

II. (e, e') SCATTERING THEORY

The inelastic electron scattering differential cross section for magnetic transitions is given by¹

$$\frac{d\sigma}{d\Omega} = \frac{Z^2 \sigma_M}{1 + 2(E_0/M_T) \sin^2(\theta/2)} \times \left[\frac{1}{2} \frac{q_\mu^2}{q^2} + \tan^2(\theta/2) \right] |F_T(q)|^2, \quad (1)$$

where Z denotes the nuclear charge, σ_M the Mott cross section, E_0 the incident electron energy, M_T the target mass, θ the scattering angle, q_μ the four momentum transferred from the electron to the nucleus, and F_T the transverse or magnetic form factor. The q_μ and the three-momentum transfer q are related by $q_\mu^2 = q^2 - \omega^2$, where ω is the difference between the incoming and outgoing electron energy. The relation between the cross section and the form factor in Eq. (1) has also been defined with Z^2 replaced by 4π .^{12,16,17}

The transverse form factor squared can be written as^{1,18}

$$|F_T(q)|^2 = \frac{4\pi}{Z^2} (2J+1) \left| \frac{q\hbar}{2Mc} \sum_\tau [\frac{1}{2} g_\tau^s \rho_{J\tau}^s(q) - 2g_\tau^l \rho_{J\tau}^l(q)] \right|^2, \quad (2)$$

where M is the nucleon mass, τ is an isospin index equal to 0 or 1, g_τ^s and g_τ^l are the spin and orbital g factors, $\rho_{J\tau}^l$ is the diagonal current transition density, and $\rho_{J\tau}^s(q)$ is the transverse spin density written as¹

$$\rho_{J\tau}^s(q) = \left[\frac{J+1}{2J+1} \right]^{1/2} \rho_{JJ-1}^{s\tau} - \left[\frac{J}{2J+1} \right]^{1/2} \rho_{JJ+1}^{s\tau}. \quad (3)$$

In a shell model picture, the $\rho_{JL}^{s\tau}$ transition density can be written as the sum of products of one-body density matrix elements and single-particle matrix elements as:¹

$$\rho_{JL}^{s\tau}(q) = \sum_{j_a j_b} Z_{J\tau}(j_a j_b) \sqrt{2\hat{j}_a \hat{j}_b}^{-1} \langle j_a \| j_L(qr) [Y_L(\hat{r}) \times \vec{\sigma}]^J \| j_b \rangle, \quad (4)$$

where $\hat{j} = \sqrt{2j+1}$, j_a is for the hole state, and j_b is for the particle state. $Z_{J\tau}$ is the "Z coefficient" given by the one-body matrix element¹⁹

$$Z_{J\tau}(j_a j_b) = \langle J_f T_f \| (a_{j_a}^\dagger \times a_{j_b})^{J,\tau} \| J_i = 0 T_i \rangle, \quad (5)$$

which has the maximum value of unity for an isoscalar or isovector pure particle-hole excitation from a closed shell.

In this work we consider $1\hbar\omega$ stretched transitions of the type $(j_b j_a^{-1}) J_{\max}$ where $J_{\max} = j_a + j_b$, $j_a = l_a + \frac{1}{2}$, $j_b = l_b + \frac{1}{2}$, $l_b = l_a + 1$, and j_a and j_b are the largest angular momenta found in the last filled shell and first open shell, respectively. This configuration is unique, if we assume that there are no contributions from $2\hbar\omega$ excitations in the ground state or from 1p-1h excitations with $E \geq 3\hbar\omega$. Of course, the stretched configurations can mix

with multinucleon-multihole configurations within the same shell. Such mixing produces physical ground and excited states that are not pure closed shell and particle-hole wave functions, respectively; however, the additional components in the wave functions will not be connected by the one-body spin and orbital current operators. The main effect is to reduce the transition strength to each state with the cross sections remaining proportional to a single-particle matrix element corresponding to the stretched configuration.

A further simplification is that the convection current transition density $\rho_{J\tau}^l$ and also $\rho_{JJ+1}^{s\tau}$ vanish as a result of angular momentum restrictions on the single-particle matrix element. Combining Eqs. (2)–(4), evaluating the reduced matrix element for the stretched particle-hole configuration, including the center of mass and nucleon finite-size corrections, and using either $\alpha=0$, 1 or $\alpha=n, p$ we get¹

$$|F_T(q)|^2 = \left| f_{\text{c.m.}} f_{fs} \frac{1}{Z} \left[\frac{q\hbar}{2Mc} \right] \left[\frac{J+1}{2J} \right]^{1/2} \hat{j}_a \hat{j}_b \langle j_a j_b \frac{1}{2} - \frac{1}{2} | J0 \rangle \frac{1}{\sqrt{2}} \sum_\alpha [C_\alpha Z_\alpha g_\alpha^s I_\alpha] \right|^2. \quad (6)$$

This uses:

$$f_{\text{c.m.}}(q) = \exp[(bq/2)^2/A],$$

$$C_\alpha = \sqrt{2} \text{ for } \alpha=0,1 \text{ and } C_\alpha=1 \text{ for } \alpha=n,p,$$

$$Z_n = (Z_0 + Z_1)/\sqrt{2} \text{ and } Z_p = (Z_0 - Z_1)/\sqrt{2} \text{ (Ref. 20),}$$

$$g_0^s = \mu_n + \mu_p, \quad g_1^s = \mu_n - \mu_p, \quad g_n^s = 2\mu_n, \text{ and } g_p^s = 2\mu_p.$$

The center-of-mass correction, $f_{\text{c.m.}}$, although based on the HO model, was used in both the HO and WS calculations. The finite-size correction, f_{fs} , was made by using the four-pole expansion of Simon *et al.*²¹ The radial integral is

$$I_\alpha(q) = \int_0^\infty \psi_{\alpha\alpha}(r) j_{J-1}(qr) \psi_{b\alpha}(r) r^2 dr. \quad (7)$$

Using the fact that $\sum_\alpha [C_\alpha Z_\alpha g_\alpha I_\alpha]$ is the same for $\alpha=0,1$, and for $\alpha=n,p$, we can write the isoscalar and isovector integrals in terms of neutron and proton integrals (since we will deal with neutron and proton states)

$$g^s I_\tau(q) = [g_n^s I_n + (-1)^\tau g_p^s I_p] / 2. \quad (8)$$

The radial integral I_α depends on the radial form of the single-particle and single-hole nucleon wave function, ψ_α . For a HO potential well the proton and neutron wave functions with the same radial quantum numbers are usually taken to have exactly the same form. In that case $I_p = I_n = I_\alpha$ and I_α has the simple form¹

$$I_\alpha = \frac{(bq)^J \exp[-(bq/2)^2]}{2^{(J-1)/2} [(J+1)!! (J-1)!!]^{1/2}}.$$

$$M_1^e = f_{\text{c.m.}} f_{\text{fs}} \frac{1}{Z} \left[\frac{q\hbar}{2Mc} \right] \left[\frac{J+1}{2J} \right]^{1/2} \hat{j}_a \hat{j}_b \langle j_a j_b \frac{1}{2} - \frac{1}{2} | J0 \rangle g_1^s I_1 \quad (11)$$

and

$$\frac{M_0^e}{M_1^e} = \frac{g_0^s I_0}{g_1^s I_1} = \frac{g_n^s I_n + g_p^s I_p}{g_n^s I_n - g_p^s I_p}. \quad (12)$$

Note that when $I_0 = I_1$, as is usually assumed when using HO wave functions, we have the ratio $M_0^e/M_1^e = -0.187$.

Using the experimental form factors and the theoretical matrix elements, we can determine Z_0 and Z_1 as fitting parameters for each stretched state. If only electron scattering data are available for a nucleus, the two Z coefficients cannot both be determined. For magnetic electron scattering, M_0^e/M_1^e is small (-0.187 when $I_0 = I_1$) and thus this reaction probes mainly the isovector transitions; we thus neglect the expected small isoscalar contribution to the cross section and from Eq. (9) we use $F^2/M_1^2 \approx (Z_1)_{\text{exp}}^2$. For $T_>$ states, only the isovector amplitude contributes, so this assumption is correct. For $T_<$ states our analysis will incorrectly yield too small a Z_1 if the Z_0/Z_1 ratio is positive and too large a Z_1 if the ratio is negative. If these constructive and destruc-

More realistically, the proton and neutron radial wave functions can be quite different as a result of Coulomb forces on the proton. Consequently, we expect to see differences in $F_T(q)$, and therefore, the form factor will take on different shapes and values depending on the specific choice of radial wave functions. In fact, the two terms in Eq. (8) should be weighted by the neutron and proton content of the transition. In cases where the transition is known to be mainly neutron or proton, $g_\tau I_\tau$ for a pure neutron or proton transition was used (see Table I). However, in other cases where the content of the transition was not known or poorly known, no weighting was used.

To emphasize the separate dependence on the reaction dynamics in M_0 and M_1 and on the nuclear structure effects in Z_0 and Z_1 , Eq. (6) can be written as

$$F^2 = (M_0^e Z_0 + M_1^e Z_1)^2$$

or

$$F^2/M_1^2 = \left[\frac{M_0^e}{M_1^e} Z_0 + Z_1 \right]^2. \quad (9)$$

Since we will mention the results of comparing electron scattering to pion scattering, we include a similar equation for pion scattering²²

$$\frac{d\sigma^\pm}{d\Omega} = (M_1^\pi)^2 \left[\frac{M_0^\pi}{M_1^\pi} Z_0 \mp Z_1 \right]^2. \quad (10)$$

The isovector M_1^e matrix element and the M_0^e/M_1^e ratio tabulated in Table I are

tive interference effects cancel over all states, however, the $\sum (Z_1)_{\text{exp}}^2$ will be correct. (If pion scattering data are also available, the Z_0/Z_1 ratio can be found by comparing π^- and π^+ cross sections. For pion scattering M_0^π/M_1^π is approximately two near the delta resonance and thus probes mainly isoscalar transitions.)

The structure effects embodied in Z_0 and Z_1 are difficult to predict for individual states, although calculations have been done for ^{14}C , ^{26}Mg , and ^{54}Fe (Refs. 22 and 23). Upper limits for the Z coefficients can, however, be determined from simple nuclear models. These sum rules can be found for $T_<$ states (where the magnetic transition, $T_i \rightarrow T_f$, is for nuclear states of isospin $T_0 \rightarrow T_0$), for $T_>$ states (where the transition is for $T_0 \rightarrow T_0 + 1$), and for the sum of the two.

The method we use for including structure effects is given by Holtkamp *et al.*²⁰ Here we define n_n and n_p as the number of neutrons and protons in the orbital j_a , and n as the total number of nucleons in that orbital. First, we look at a $T_>$ stretched transition of multipolarity J induced by an isovector one-body operator to a state which has the form $|\text{core}\rangle_0 + \times |j_a^{n-1} j_b\rangle_J$, where

TABLE I. Listed here are the results of the present analysis comparing experimental form factors [F^2 as defined in Eq. (1)] to theoretical matrix elements [M_1^2 as calculated from Eq. (11)]. No MEC effects have been included. A least squares fit was used to match the theory to all the experimental data points, although theoretical values at only the peak of the curve are listed in this table. The binding energies used in the calculations are listed for each stretched state. Where only one binding energy is listed for a state, it was treated as a pure neutron or proton transition in Eq. (8). Note that the 19.5 MeV state in ^{12}C has mixed isospin. The M_0/M_1 ratio from WS wave functions is calculated using Eq. (12), whereas $M_0/M_1 = -0.187$ when HO wave functions are used. Sums of $(Z_1)_{\text{exp}}^2$ for each nuclide and comparison with theory are given in Table III. The energies in the table have units of MeV; all other quantities are unitless.

T	State	Binding energy		$M_1^2 (\times 10^{-5})$			M_0^2/M_1^2 (WS)	$F^2/M_1^2 \approx (Z_1)_{\text{exp}}^2$	
		n	p	(HO)	(WS)	(WS/HO)		(HO)	(WS)
				$^{12}\text{C } J^\pi = 4^- (j_a = \frac{3}{2}^- j_b = \frac{5}{2}^+) \text{ Ref. 24}$					
	19.5	+0.78	+3.54	264.0	113.0	0.43	-0.248	0.422	1.045
				$^{14}\text{C } J^\pi = 4^- (j_a = \frac{3}{2}^- j_b = \frac{5}{2}^+) \text{ Ref. 25}$					
<	11.7	-0.16		257.0	164.0	0.64	-0.187	0.0871	0.105
<	17.3		-3.53	257.0	216.0	0.84	-0.187	0.102	0.104
>	24.4	+1.11	+3.57	257.0	119.0	0.46	-0.195	0.215	0.424
				$^{16}\text{O } J^\pi = 4^- (j_a = \frac{3}{2}^- j_b = \frac{5}{2}^+) \text{ Ref. 26}$					
<	17.8	-4.05	-0.66	136.0	105.0	0.77	-0.173	0.0161	0.0199
>	17.9	-3.96	-0.57	136.0	104.0	0.76	-0.173	0.0226	0.0280
>	18.6	-3.21	+0.18	136.0	88.7	0.65	-0.116	0.0334	0.0489
>	19.0	-2.87	+0.52	136.0	87.1	0.64	-0.115	0.411	0.618
<	19.8	-2.04	+1.35	136.0	82.4	0.61	-0.111	0.0003	0.0004
>	20.5	-1.33	+2.06	136.0	78.6	0.58	-0.111	0.0539	0.0921
				$^{24}\text{Mg } J^\pi = 6^- (j_a = \frac{5}{2}^+ j_b = \frac{7}{2}^-) \text{ Ref. 17}$					
>	15.0	-1.94	+2.91	47.8	34.8	0.73	-0.111	0.195	0.247
				$^{26}\text{Mg } J^\pi = 6^- (j_a = \frac{5}{2}^+ j_b = \frac{7}{2}^-) \text{ Ref. 23}$					
<	7.5	-3.55	-6.60	48.2	45.5	0.94	-0.216	0.0030	0.0025
<	9.2	-1.92	-4.97	48.2	44.0	0.91	-0.221	0.0325	0.0324
<	12.5	+1.41	-1.64	48.2	36.4	0.76	-0.301	0.0417	0.0533
<	12.9	+1.79	-1.26	48.2	35.9	0.74	-0.301	0.0189	0.0246
<	13.0	+1.91	-1.14	48.2	36.0	0.75	-0.298	0.0101	0.0133
<	14.0	+2.88	-0.17	48.2	34.6	0.72	-0.306	0.0152	0.0193
<	14.5	+3.41	+0.36	48.2	29.3	0.61	-0.243	0.0230	0.0380
<	15.4	+4.27	+1.22	48.2	29.2	0.61	-0.234	0.0246	0.0416
<	15.5	+4.37	+1.32	48.2	29.4	0.61	-0.224	0.0444	0.0765
<	16.5	+5.41	+2.36	48.2	29.2	0.61	-0.208	0.0535	0.0865
>	18.0	-0.83	+3.90	48.2	32.7	0.68	-0.112	0.146	0.220
				$^{28}\text{Si } J^\pi = 6^- (j_a = \frac{5}{2}^+ j_b = \frac{7}{2}^-) \text{ Ref. 12}$					
>	14.4	-2.81	+2.78	35.3	25.4	0.72	-0.110	0.330	0.427
				$^{48}\text{Ca } J^\pi = 8^- (j_a = \frac{7}{2}^- j_b = \frac{9}{2}^+) \text{ Ref. 16}$					
<	9.1	-0.80		14.2	13.0	0.92	-0.187	0.0249	0.0266
<	9.3	-0.66		14.2	12.9	0.91	-0.187	0.0752	0.0803
<	10.0	+0.04		14.2	9.79	0.69	-0.187	0.0268	0.0383
				$^{54}\text{Fe } J^\pi = 8^- (j_a = \frac{7}{2}^- j_b = \frac{9}{2}^+) \text{ Ref. 27}$					
<	8.3	-5.07	-0.54	8.26	8.25	1.00	-0.191	0.0301	0.0294
<	8.9	-4.43	+0.10	8.26	6.96	0.84	-0.123	0.0358	0.0418
<	10.0	-3.41	+1.12	8.26	6.90	0.84	-0.126	0.0330	0.0383
<	10.7	-2.67	+1.83	8.26	6.19	0.75	-0.187	0.0358	0.0471
>	13.3	-4.38	+4.41	8.26	6.82	0.83	-0.115	0.159	0.190
				$^{58}\text{Ni } J^\pi = 8^- (j_a = \frac{7}{2}^- j_b = \frac{9}{2}^+) \text{ Ref. 28}$					
<	7.9	-3.21	+0.99	7.02	5.90	0.84	-0.129	0.0443	0.0515
<	8.8	-2.34	+1.86	7.02	5.85	0.83	-0.133	0.0485	0.0573
>	10.2	-5.34	+3.24	7.02	5.95	0.85	-0.118	0.0305	0.0354
>	11.2	-4.29	+4.29	7.02	5.87	0.84	-0.119	0.0478	0.0565
>	12.5	-3.03	+5.55	7.02	5.78	0.82	-0.122	0.0859	0.103

TABLE I. (Continued.)

T	State	Binding energy		$M_1^2 (\times 10^{-5})$			M_0^i/M_1^i (WS)	$F^2/M_1^2 \approx (Z_1^i)_{\text{exp}}^2$	
		n	p	(HO)	(WS)	(WS/HO)		(HO)	(WS)
$^{60}\text{Ni } J^\pi = 8^- (j_a = \frac{7}{2}^- \quad j_b = \frac{9}{2}^+) \text{ Ref. 11}$									
<	7.5	-7.77	-2.01	6.97	7.18	1.03	-0.188	0.0497	0.0476
<	8.4	-6.86	-1.12	6.97	7.10	1.02	-0.187	0.0199	0.0192
<	9.0	-6.28	-0.57	6.97	7.06	1.01	-0.187	0.0262	0.0258
<	9.2	-6.12	-0.36	6.97	7.04	1.01	-0.187	0.0244	0.0240
>	12.3	-6.41	+2.80	6.97	5.98	0.86	-0.117	0.0155	0.0181
>	12.5	-6.24	+2.97	6.97	5.97	0.86	-0.117	0.0266	0.0311
>	13.9	-4.83	+4.38	6.97	5.85	0.84	-0.118	0.0448	0.0529
>	14.8	-3.90	+5.31	6.97	5.74	0.82	-0.116	0.0300	0.0363
>	15.5	-3.24	+5.97	6.97	5.65	0.81	-0.115	0.0238	0.0289
>	16.1	-2.66	+6.55	6.97	5.57	0.80	-0.115	0.0107	0.0131
$^{90}\text{Zr } J^\pi = 10^- (j_a = \frac{9}{2}^+ \quad j_b = \frac{11}{2}^-) \text{ Refs. 29 and 1}$									
<	7.4	-4.61		2.99	3.16	1.06	-0.187	0.259	0.246
$^{208}\text{Pb } J^\pi = 14^- (j_a = \frac{13}{2}^+ \quad j_b = \frac{15}{2}^-) \text{ Ref. 30}$									
<	6.7	-2.26		0.579	0.657	1.13	-0.187	0.179	0.163

$J = j_a + j_b = 2j_a + 1$ for a stretched state. Then the square of the isovector Z coefficient summed over all observed transitions is given by²⁰

$$\sum_i (Z_1^i)_{\text{thr}}^2 = \frac{1}{2J} \left[\frac{2}{T_0 + 1} n_p \right], \text{ for } T_>. \quad (13)$$

The sum rule is also valid when the ground state (or excited state) contains admixtures of other orbital configurations such as j_c^n so long as $j_c + j_a < J$. The maximum value of the sum occurs when n is evaluated in the extreme single-particle shell model as above, and this is used as our standard for comparison.

For $T_<$ stretched magnetic transitions, the maximum isovector strength is given by²⁰

$$\sum_i (Z_1^i)_{\text{thr}}^2 = \frac{1}{2J} \left[n_n + \left[\frac{T_0 - 1}{T_0 + 1} \right] n_p \right], \text{ for } T_<. \quad (14)$$

The sum of the two gives

$$\sum_i (Z_1^i)_{\text{thr}}^2 = \frac{1}{2J} [n_n + n_p] = \frac{n}{2J}, \text{ for } T_{\text{tot}}. \quad (15)$$

Note that in general $2n_n = 2n_p = n = 2J$ for a full orbital. Equation (15) is also true for $\sum_i (Z_0^i)_{\text{thr}}^2$.

III. CALCULATING WAVE FUNCTIONS AND FORM FACTORS

We will treat $M4$ excitations in ^{12}C ,²⁴ ^{14}C ,²⁵ and ^{16}O ,²⁶ $M6$ excitations in ^{24}Mg ,¹⁷ ^{26}Mg ,²³ and ^{28}Si ,¹² $M8$ excitations in ^{48}Ca ,¹⁶ ^{54}Fe ,²⁷ ^{58}Ni ,²⁸ and ^{60}Ni ,¹¹ one $M10$ excitation in ^{90}Zr ,²⁹ and one $M14$ excitation in ^{208}Pb .³⁰ A range of both bound and unbound excitations is treated for each nucleus, matching those states examined by electron scattering.

Form factors have usually been calculated using HO wave functions. Fits to the experimental momentum-transfer dependence q for each transition are obtained by

varying the length parameter b . This χ^2 fitting procedure was redone here, varying the b and the normalization. The “best fit” value of b for each nucleus is listed in Table II. The value listed is the same within uncertainties as has been previously found.

In this paper we use WS wave functions, in which case there are more input variables to adjust. Here we discuss the binding energies and potential parameters used to calculate hole- and particle-state wave functions and the sensitivity of M_1^2 to these choices.

As is usual, the binding energy (E_B) of the hole state is assumed to be the separation energy (E_S) of the nucleon in that state, and the binding energy of the particle state is that for the hole state plus the excitation energy (E_E) of the stretched state. Although other schemes may be considered, the results are highly insensitive to this assumption. For simplicity all hole states and particle states use the same WS potential geometry.

For many of the nuclei, the ground state of the $(A - 1)$ nucleus does not have the proper spin j_a and isospin. When the ground state does not have the proper spin, the excitation energy (E_J) of the lowest state in the $(A - 1)$ nucleus with the proper spin is added to the separation energy. The case where the ground state does not have proper isospin is for $T_>$ stretched states in $(N - 1)$ nuclei where $T_0 \neq 0$. For these $T_> = T_0 + 1$ stretched states, the proper isospin of the neutron hole state or particle state is $T_0 + \frac{1}{2}$, since this is the only decay allowed if the isospin rules are strictly obeyed. Because isospin rules are not strictly obeyed, however, the neutron state should be weighted by the lower isospin $T_0 - \frac{1}{2}$ also. In our calculations for the particle state, the excitation energy (E_T) of only the state with proper isospin was added to the separation energy. For the hole state, however, very little sensitivity to the binding energy of the hole state was found, so for simplicity, no adjustment was made for the proper isospin. The binding energies can then be written as $E_{B,\text{hole}} = -E_S - E_J$ and $E_{B,\text{part}} = E_E - E_S - E_J$. This

TABLE II. The parameters listed here were used in calculating the wave functions for the best χ^2 fit. The b is the oscillator length for calculating HO wave functions. The potential used in calculating the WS wave functions is $U = -V_0 f + V_0 \lambda (\hbar/2m_\pi c)^2 (m_\pi/M)^2 (\sigma \cdot l) r^{-1} df/dr$, where $f = \{1 + \exp[(r - r_0 A^{1/3})/a]\}^{-1}$; $(m_\pi/M)^2 = 1/45.2$, and $V_0 \lambda/45.2 = V_{s.o.}$. A Coulomb radius of $r_c = 1.25 \times A^{1/3}$ fm was used for all nuclei. The "fit" values were used for the calculations in Table I and the plots in Fig. 4. The final column shows how much the experimental $\sum(Z_1)_{\text{exp}}^2$ in Table III changes if potential parameters from the literature are used instead of the "fit" parameters.

Nucleus	b (fm)	r_0 (fm)	a (fm)	$\lambda/V_{s.o.}$ (MeV)	Ref.	$\sum(Z_1)^2/\sum(Z_1)_{\text{fit}}^2$
^{12}C	1.52±0.03	1.01±0.04	0.65	$\lambda=25$	fit	1.0
		1.20	0.65	$V_{s.o.}=24$	35	1.39
		1.25	0.5	$V_{s.o.}=24$	24	1.14
^{14}C	1.49±0.06	0.84±0.11	0.65	$\lambda=25$	fit	1.0
		1.16	0.78	$\lambda=25$	38 ^a	0.94
		1.25	0.5	$V_{s.o.}=24$	23	0.91
^{16}O	1.55±0.04	0.96±0.06	0.65	$\lambda=25$	fit	1.0
		1.23	0.6	$V_{s.o.}=24$	35	1.27
		1.22	0.6	$V_{s.o.}=29$	26	1.27
^{24}Mg	1.83±0.04	1.30±0.04	0.65	$\lambda=25$	fit	1.0
		1.25	0.65	$\lambda=25$	39	0.99
^{26}Mg	1.76±0.06	1.21±0.07	0.65	$\lambda=25$	fit	1.0
		1.25	0.65	$\lambda=25$	39	1.07
		1.42	0.5	$V_{s.o.}=24$	23	1.12
^{28}Si	1.73±0.02	1.16±0.02	0.65	$\lambda=25$	fit	1.0
		1.25	0.65	$\lambda=25$	40	1.07
		1.20	0.65	$\lambda=25$	41	1.04
^{48}Ca	1.92±0.04	1.24±0.04	0.65	$\lambda=25$	fit	1.0
		1.17	0.65	$V_{s.o.}=28$	34	0.80
^{54}Fe	1.91±0.03	1.22±0.02	0.65	$\lambda=25$	fit	1.0
		1.23	0.65	$V_{s.o.}=28$	34	1.01
^{58}Ni	1.93±0.05	1.19±0.04	0.65	$\lambda=25$	fit	1.0
		1.11	0.65	$V_{s.o.}=24$	35	0.88
^{60}Ni	1.95±0.04	1.22±0.03	0.65	$\lambda=25$	fit	1.0
		1.11	0.65	$V_{s.o.}=24$	35	0.88
		1.17	0.65	$V_{s.o.}=28$	34,37	0.96
^{90}Zr	2.08±0.04	1.26±0.03	0.65	$\lambda=25$	fit	1.0
		1.27	0.65	$V_{s.o.}=28$	34	1.00
^{208}Pb	2.23±0.04	1.18±0.02	0.65	$\lambda=25$	fit	1.0
		1.20	0.65	$V_{s.o.}=28$	34	1.00

^aBinding parameters were misprinted.

changes to $E_{B,\text{part}} = E_E - E_S - E_T$ for the neutron binding energy in $T_>$ stretched states in $T_0 \neq 0$ nuclei. See Table I for the binding energies for each state.

We now discuss how the results differ depending on what isospin state is used for the special case mentioned above. The $T_>$ stretched states in nuclei where $T_0 \neq 0$ are the 24.4 MeV state in ^{14}C , the 18.0 MeV state in ^{26}Mg , the 13.3 MeV state in ^{54}Fe , three states in ^{58}Ni , and six states in ^{60}Ni . The particle state shows a definite sensitivity to the isospin used. If the proper upper isospin is used, the neutron in all the above states is bound except the one in ^{14}C , whereas, if the lower isospin is used only the neutron in the state in ^{54}Fe is bound. Any kind of weighting of the two isospin states decreases the calculated M_1^2 from what we use in Table I, and if only the lower isospin is used the decrease is up to 20% for any individual state. The 24.4 MeV 4^- state in ^{14}C was too unbound when the lower isospin was used and our method failed to converge. The hole state, on the other hand, shows very little sensitivity to the isospin used. For example, the $T = \frac{3}{2} f_{7/2}$ neutron hole state in ^{59}Ni has a

binding energy of -15.29 MeV [$E_{S,n} = 11.389$ MeV and $E_J = 3.9$ MeV (Ref. 31)], while the $T = \frac{5}{2} f_{7/2}$ hole state has a binding energy of -18.74 MeV [$E_{S,n} = 11.389$ MeV and $E_T = 7.35$ MeV (Ref. 32)]. The calculated M_1^2 computed with these two extremes differ by less than 1%.

For unbound states we used the option in the computer code DWUCK4 (Ref. 13) which treats the unbound level as a resonance.¹⁴ The unbound wave function is normalized by forcing it and its derivative to be zero at the radius picked for the limit of integration. This method is commonly used for computing the appropriate wave functions for a nucleon stripping reaction.

The radial integrations were performed with a step size of 0.1 fm and a maximum outer radius of 40 fm. This was found to be adequate to obtain stability in the predicted decay-particle widths. For the 14.4 MeV $T = 1$ state in ^{28}Si the method we use yields a single-particle proton width of 10.5 keV which is close to the 10.8–17.4 keV range of widths found by Nelson *et al.*³³ in comparing R -matrix and g -matrix methods in detail. (They give $\Gamma_{s.p.} = 11.9$ keV.) This comparison demonstrates the reli-

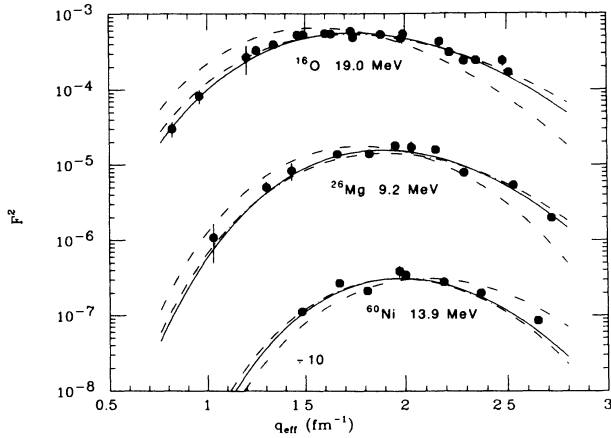


FIG. 1. The results of using different potential well parameters in calculating the theoretical form factors are shown for states in three nuclei. The solid curves show the HO "fit" and the single-dot-dashed curves show the WS "fit." The double-dot-dashed curves use other parameters: ^{16}O from Ref. 35, ^{26}Mg from Ref. 23, and ^{60}Ni from Ref. 35.

ability of our method. For the 24.4 MeV $T=2$ state in ^{14}C our method yields a single-particle proton width of 0.59 MeV when the allowed isospin decay is used. This state has an observed width of 1.7 MeV,²⁰ which is the broadening expected if some decay to the lower isospin daughter is present.

The shape parameters for the potentials may be determined by elastic magnetic electron scattering from the valence nucleon; these parameters have been determined

in several cases.^{34,35} It is also advantageous to use the same potential well to generate wave functions for stripping reactions and for magnetic electron scattering,³⁶ thus, we include several examples of stripping parameters.³⁷⁻⁴⁰ This should yield a more consistent comparison between the two classes of reactions. We also include shape parameters determined for scattering to stretched states in three cases.^{24,26,41} Since the parameters that describe the potential for the final state cannot be determined by any independent means, some freedom exists and, consequently, some ambiguity in the predictions is encountered. One way to choose the parameters would be to use the previously determined ground-state geometrical parameters to generate the hole wave functions and to vary only the parameters for the particle wave functions. However, our results show little sensitivity to the hole state parameters, and for simplicity we maintain the same parameters for both the particle and the hole states.

A χ^2 fitting procedure was done by varying r_0 and the normalization Z_1^2 . The diffuseness a and the spin-orbit parameter λ were kept constant at 0.65 fm and 25 fm, respectively (although the fit for ^{14}C could be improved by a larger diffuseness of 0.8 fm). The "best fit" value of r_0 for each nucleus is listed in Table II. Other values of r_0 used previously are listed in Table II for comparison. The results of using these different r_0 are shown for several nuclei in Fig. 1. The HO curve is shown along with two WS curves. All calculations shown in Fig. 1 have been normalized to the magnitude of the data. The value found for r_0 in our analysis is comparable to previous values except for ^{12}C , ^{14}C , and ^{16}O , where our value is smaller than before.

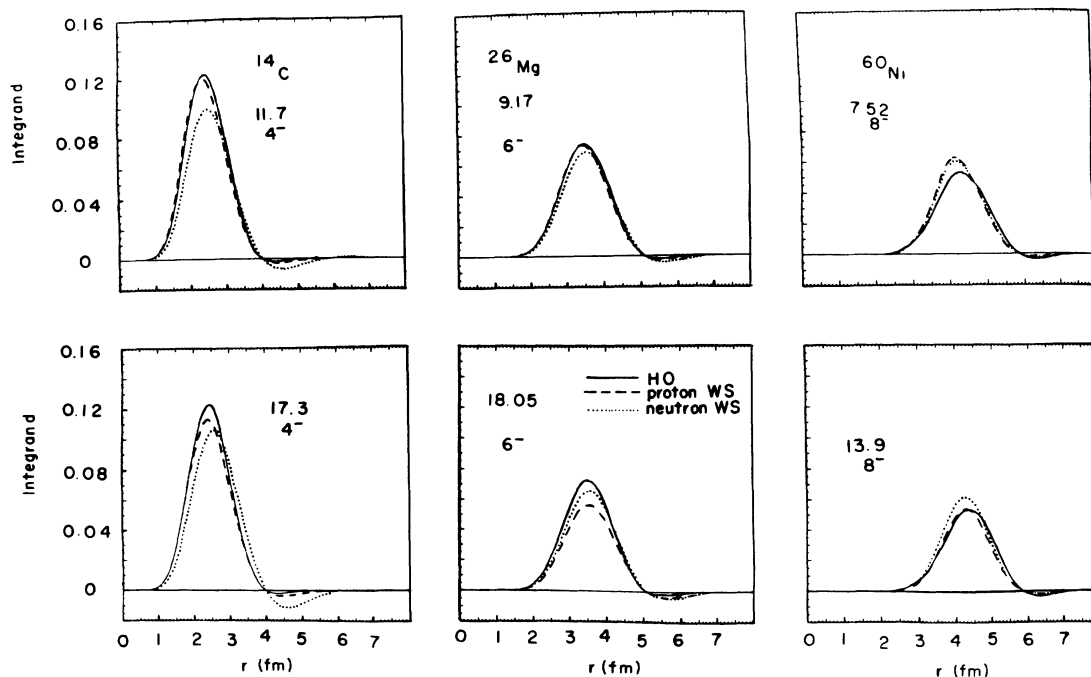


FIG. 2. The integrand of the radial integral at the maximum on the theoretical form factor curve for two states each in ^{14}C ($q_{\text{max}} = 1.70 \text{ fm}^{-1}$), ^{26}Mg ($q_{\text{max}} = 1.90 \text{ fm}^{-1}$), and ^{60}Ni ($q_{\text{max}} = 2.00 \text{ fm}^{-1}$). The states plotted in each nucleus are the two most extreme stretched states for which there are good data for comparison.

There have been other references suggesting the need for using smaller radii. Although the ground state of ^{13}C is not the hole state for stretched excitations in ^{14}C , it is interesting to note that a value of $r_0=0.9$ fm for ^{13}C is given by Donnelly and Sick³⁵ as the best fit to the magnetic elastic data. In a recent reference that calculates the mean field for negative and positive energy neutrons in ^{208}Pb , the radius of the real potential was found to decrease for more positive (unbound) single-particle energies, and for more negative (deeply bound) single-hole energies.⁴² This decrease in radius amounted to about 3% at ± 10 MeV, however, which is much less than the decrease in radius (from the radii found for ground-state distributions) detailed in Table II of about 20%, even for states close to the nucleon binding energy.

To understand better how the matrix elements are dependent on the wave functions used, we have plotted in Fig. 2 the integrand of the radial integral [see Eq. (7)] for several states. These were evaluated at a value of q where the matrix element is a maximum. The less bound nucleon extends to a larger radius, and thus the overlap of the particle and the hole states decreases, yielding smaller matrix elements. This is particularly true for the final states at higher energies, as seen for ^{26}Mg and ^{60}Ni . The results in Table I are the clear result of the amount of

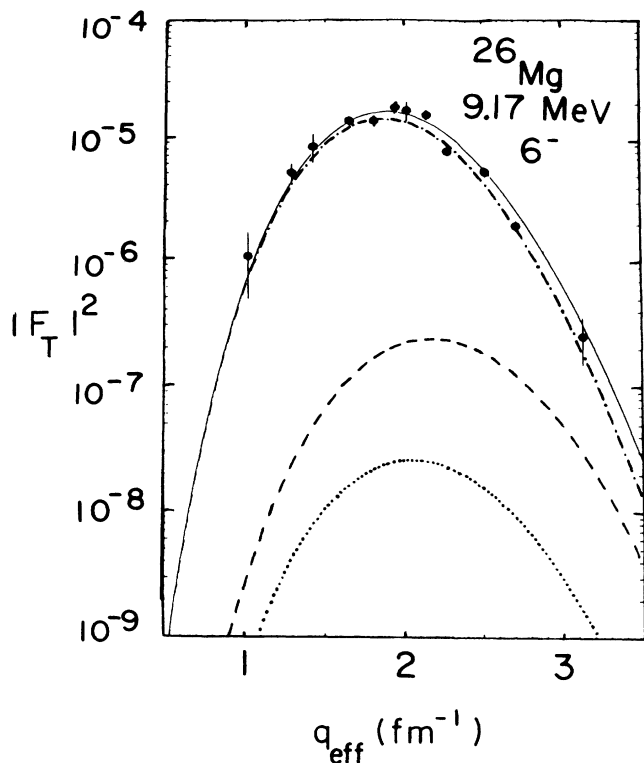


FIG. 3. The results of including meson exchange current (MEC) effects are shown for the 9.17 MeV state in ^{26}Mg . The data are to be compared with the solid line which includes MEC effects. These effects are made up of the non-MEC term (dot-dashed line), the seagull term (dashed line), and the pionic term (dotted line). The curves can be assumed to come from either HO or WS wave functions.

overlap seen in Fig. 2.

The effect of meson exchange currents (MEC) was also computed, and the influence of WS and HO wave functions was compared. The expressions of Dehesa *et al.*^{15,43} were evaluated with both sets of wave functions for the isovector mode. The entire ensemble of initial states (not just that for the hole state) was computed using the WS potential. The results of including MEC effects are shown in Fig. 3 where ^{26}Mg is used as an example. This figure includes the curves for the seagull and pionic terms which enter with opposite signs. The effect is the same to within 3% (usually 1%) whether HO or WS wave functions are used. The inclusion of MEC effects increases the theoretical predictions between 15 and 20%. This would decrease yet further the fractions of single-particle strength obtained by comparing data to calculations, as shown previously.¹⁰ The results shown here will not include MEC effects.

IV. RESULTS

In Fig. 4 theoretical form factors calculated from both HO and WS wave functions are compared to some representative electron scattering data. For several states the WS matrix elements were calculated separately for neutrons and protons and these are included in Fig. 5. Neutron and proton WS curves were each normalized to the data by the same factor as was the combined WS curve. For the states in Fig. 5 where neutron and proton matrix elements were plotted, we notice the results of isospin asymmetry. As expected, the theoretical form factor is smaller for the less bound nucleon as already discussed for Fig. 2.

Using HO wave functions with a constant b results in the theoretical form factor peaking at the same momentum transfer q_{max} for all stretched states. When the value of b is allowed to vary from state to state, as in ^{60}Ni for example, the variation in b is ± 0.02 fm with no systematic dependence on the excitation energy. When WS wave functions are used instead, the stretched states at higher excitation energies have wave functions that extend further out and the theoretical form factor peaks at a smaller q_{max} . However, this change in q_{max} between the lowest and highest stretched state of a given nucleus is in general only 0.03 fm^{-1} or less. In the extreme case of ^{26}Mg the 18.0 MeV state peaks 0.07 fm^{-1} lower than the 7.5 MeV state, but even this shift is difficult to detect in the data.

Table I gives the results of the analysis using WS wave functions and compares these to results using HO wave functions. The HO theoretical matrix elements have not taken into account the excitation energy of the state, whereas the WS matrix elements have. As a result, the HO form factor curves are the same for all states for the constant value of b used for each target. The ratio between WS and HO calculations shows that the theoretical M_1^2 for WS wave functions decreases with respect to HO wave functions as the excitation energy increases. The ratio abruptly decreases at energies where a nucleon becomes unbound. This is as expected since the overlap between initial and final wave functions decreases; this

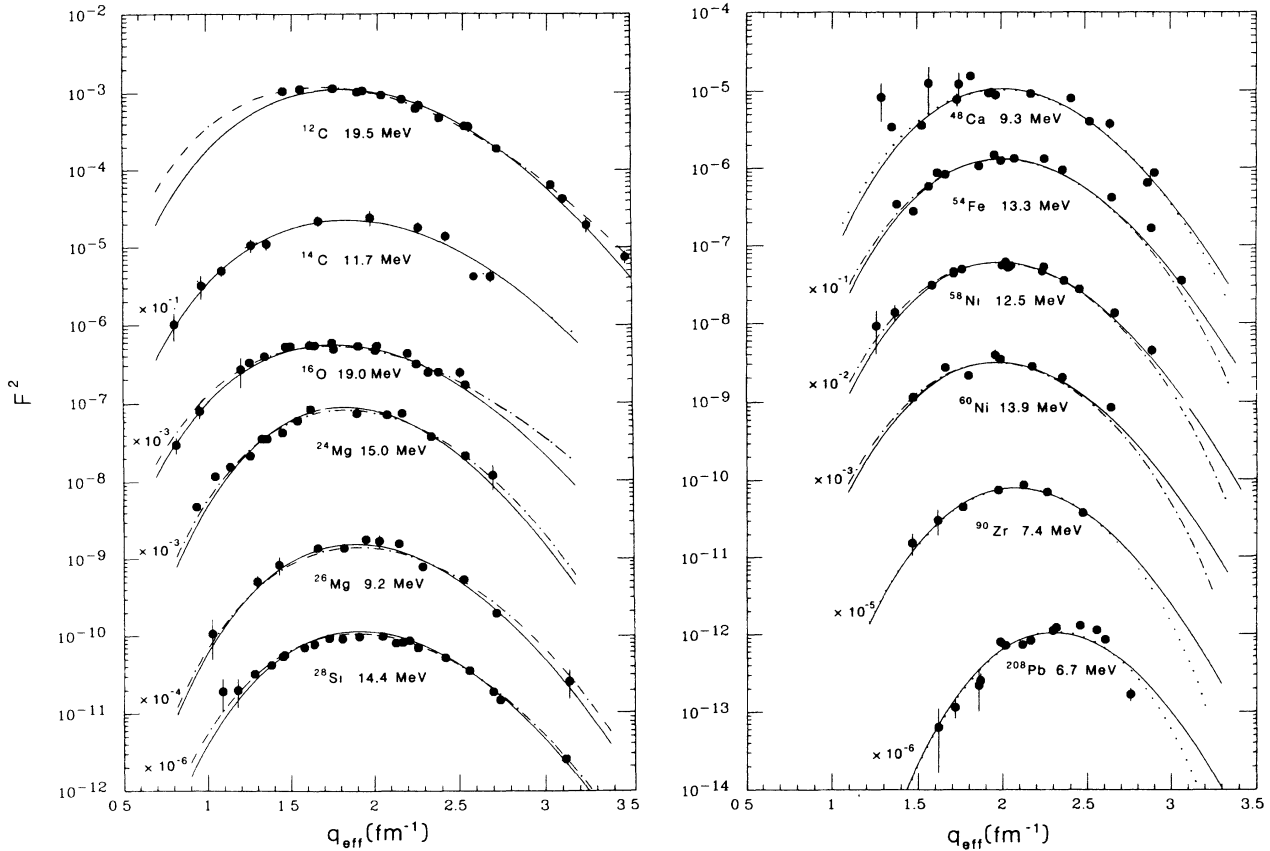


FIG. 4. Electron scattering data are here compared to predictions. Solid curves use HO wave functions and dot-dashed curves use WS wave functions. The magnitudes of the theoretical curves have been normalized to the data. These plots do not include MEC effects. For ^{14}C , ^{48}Ca , ^{90}Zr , and ^{208}Pb the (dotted) curves use only the neutron part of the WS wave function.

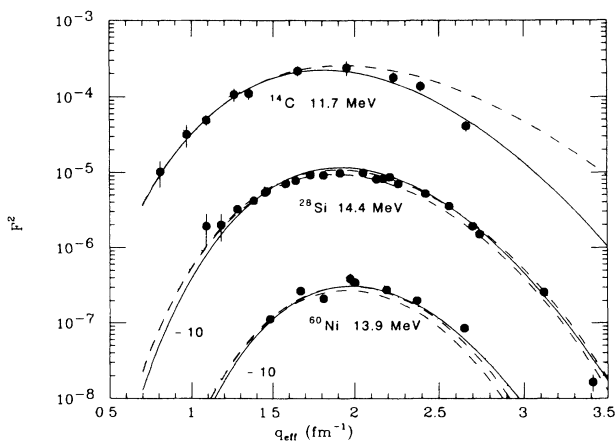


FIG. 5. Electron scattering data compared to predictions as in Fig. 4, but with neutron (dotted curve) and proton (dashed curve) WS wave functions shown separately. The solid curves use HO wave functions and the dot-dashed curves use (total) WS wave functions. The magnitudes of the theoretical curves have been normalized to the data. No total WS curve is given for ^{14}C because the 11.7 MeV state is the result of a neutronlike transition.

effect was also pointed out by Siciliano and Weiss.⁴⁴ The M_0/M_1 ratio from WS wave functions is in many cases much different than -0.187 . Again, the ratio changes abruptly when the nucleon becomes unbound. In some cases the ratio is as large as -0.3 at the peak of the curve and as large as -1 above $q_{\text{eff}} = 3.5 \text{ fm}^{-1}$. This could make neglect of the isoscalar term a poor approximation. The ratios M_0^e/M_1^e and F^2/M_1^2 can be used in conjunction with pion scattering data to calculate Z_0 and Z_1 by solving Eqs. (9) and (10) simultaneously. The resulting changes in Z_1 are discussed in the next section.

The sums of F^2/M_1^2 from Table I are given in Table III for $T_<$ states, $T_>$ states, and the total. The isospin assignments in the literature are assumed to be correct, although untested in most cases. The $(Z_1)_{\text{thr}}^2$ in Table III are calculated using Eqs. (13)–(15). Experimental data are compared to theoretical predictions for $T_<$ and $T_>$ states separately, as well as the total. Using WS wave functions, the ^{12}C data exhaust 105% of the sum expected and the ^{16}O data exhaust 81%. These would be 15–20% smaller if MEC effects had been included. In general the data exhaust a large fraction of the sum rule for light nuclei, but exhaust a decreasing amount for heavier nuclei. Also listed are the comparisons between

TABLE III. Sums of $(Z_1)_{\text{exp}}^2$ from Table I for each nuclide are listed as $\sum(Z_1)_{\text{exp}}^2$. Theory calculations use Eqs. (13), (14), and (15) for $\sum(Z_1)_{\text{thr}}^2$. Note that ^{48}Ca , ^{90}Zr , and ^{208}Pb are pure neutron transitions. The HO results are in agreement with those presented previously where comparisons to previous extreme single-particle model calculations could be made.

Nuclide, J^π	T	$\sum[F^2/M_1^2 \approx (Z_1)_{\text{exp}}^2]$		$\sum(Z_1)_{\text{thr}}^2$	$\sum(Z_1)_{\text{exp}}^2 / \sum(Z_1)_{\text{thr}}^2$		
		(HO)	(WS)		(HO)	(WS)	(WS/HO)
^{12}C 4 ⁻	<			0			
	>	0.422	1.045	1	42%	105%	
	total	0.422	1.045	1	42%	105%	2.48
^{14}C 4 ⁻	<	0.189	0.208	$\frac{1}{2}$	38%	42%	
	>	0.215	0.424	$\frac{1}{2}$	43%	85%	
	total	0.404	0.632	1	40%	63%	1.56
^{16}O 4 ⁻	<	0.016	0.020	0			
	>	0.521	0.787	1	52%	79%	
	total	0.537	0.807	1	54%	81%	1.50
^{24}Mg 6 ⁻	<			$\frac{1}{3}$	0%	0%	
	>	0.195	0.247	$\frac{1}{3}$	58%	74%	
	total	0.195	0.247	$\frac{2}{3}$	29%	37%	1.27
^{26}Mg 6 ⁻	<	0.267	0.388	$\frac{1}{2}$	53%	78%	
	>	0.146	0.220	$\frac{1}{3}$	44%	66%	
	total	0.413	0.608	$\frac{5}{6}$	50%	73%	1.47
^{28}Si 6 ⁻	<			0			
	>	0.330	0.427	1	33%	43%	
	total	0.330	0.427	1	33%	43%	1.29
^{48}Ca 8 ⁻	<	0.127	0.145	$\frac{1}{2}$	25%	29%	
	>			0			
	total	0.127	0.145	$\frac{1}{2}$	25%	29%	1.14
^{54}Fe 8 ⁻	<	0.135	0.156	$\frac{1}{2}$	27%	31%	
	>	0.159	0.190	$\frac{3}{8}$	42%	51%	
	total	0.294	0.346	$\frac{7}{8}$	34%	40%	1.18
^{58}Ni 8 ⁻	<	0.093	0.109	$\frac{1}{2}$	19%	22%	
	>	0.164	0.195	$\frac{1}{2}$	33%	39%	
	total	0.257	0.304	1	26%	30%	1.18
^{60}Ni 8 ⁻	<	0.120	0.117	$\frac{2}{3}$	18%	18%	
	>	0.152	0.180	$\frac{1}{3}$	46%	54%	
	total	0.272	0.297	1	27%	30%	1.09
^{90}Zr 10 ⁻	<	0.259	0.246	$\frac{1}{2}$	52%	49%	
	>			0			
	total	0.259	0.246	$\frac{1}{2}$	52%	49%	0.95
^{208}Pb 14 ⁻	<	0.179	0.163	$\frac{1}{2}$	36%	33%	
	>			0			
	total	0.179	0.163	$\frac{1}{2}$	36%	33%	0.91

HO and WS calculations for each nucleus. The WS calculations strongly enhance the amount exhausted for light nuclei compared to HO calculations, but leave approximately unchanged the amount exhausted for heavier nuclei.

V. DISCUSSION

The distinction between results with HO and WS wave functions is most dramatic for the light nuclei, diminish-

ing for heavier nuclei. This can possibly be understood in terms of the increasing role of the centrifugal potential term retarding the extension of the unbound radial wave function. Using $R = 1.1 \times A^{1/3}$ fm and l for the particle state, this potential

$$V_l = \frac{l_b(l_b + 1)\hbar^2}{2MR^2}$$

is 18, 22, 24, 26, and 27 MeV for ^{14}C , ^{28}Si , ^{54}Fe , ^{90}Zr , and

^{208}Pb , respectively. The particle angular momentum increases faster than does the nuclear size, decreasing the decay probability and decreasing the binding energy effects for heavier nuclei.

Several comments can be made about the fraction of the sum rule strength exhausted by the data in Table III. Including MEC effects decreases all fractions by 15–20%. Including the ground-state isospin when calculating $T_>$ state wave functions in $T_0 \neq 0$ nuclei could increase the fraction of the sum rule up to 20%. Using the larger r_0 (near 1.2 fm), as listed in the literature for ^{12}C , ^{14}C , and ^{16}O , could substantially increase the fraction of the sum rule in some cases as seen in Table II.

For nuclei on which pion scattering has been done, the results of including isoscalar transition effects in Eq. (9) can be seen in several cases. (These effects will be independent of whether HO or WS wave functions are used.) The Z_0/Z_1 ratio can be calculated directly from the pion scattering σ^+/σ^- ratio with no need to assume any particular wave function. Using the Z_0/Z_1 ratios from the literature, the fraction of the total sum strength changes by less than 2% for ^{14}C ,^{20,23} ^{16}O ,⁴⁵ ^{28}Si ,⁴⁵ and ^{54}Fe .²² For the isospin mixed 19.5 MeV state in ^{12}C , $|Z_0| = 0.62$ and $|Z_1| = 0.57$.²⁴ Depending on whether the ratio of Z_0/Z_1 is negative or positive, the fraction will decrease by a factor of 0.62 or increase by a factor of 1.9, respectively. For the neutron transitions in ^{48}Ca , ^{90}Zr , and ^{208}Pb , $Z_0/Z_1 = 1$, in which case the fraction will increase by a factor of 1.5.

An analysis of pion scattering to stretched states using WS wave functions (especially for unbound states) should be even more revealing than this analysis of electron scattering. The electromagnetic probe interacts with the whole nuclear volume, but the strongly absorbed pion is particularly sensitive to the nuclear surface. In neutron excess nuclei such as ^{14}C the neutron component of the transition density extends beyond the proton component and enhances negative pion scattering. This effect has been demonstrated for giant quadrupole resonances,⁴⁶ but shown to be slight for the nearly bound stretched state of isosymmetric ^{12}C .⁴⁴ An analysis using WS wave functions is now in progress on new $^{60}\text{Ni}(\pi, \pi')$ data as well as previously published data on other nuclei.⁴⁷

VI. CONCLUSIONS

The result of this work is a substantial increase in the fraction of the expected stretched magnetic transition strength for light nuclei when existing data are compared to new theoretical predictions. For ^{12}C and ^{16}O , the $M4$ strength fractions are increased by factors of 2.5 and 1.5, respectively. The other light nuclei also have significant increases. The increase is less dramatic for heavier nuclei, and in fact for ^{90}Zr and ^{208}Pb there is a slight decrease. It is not unreasonable to expect that unobserved weak states in these nuclei could account for the difference from 100%, or that a lack of closure of the hole orbital hampers the excitation. A recent calculation of the quenching expected with a momentum-dependent residual particle-hole interaction found quenching effects of 10–20% (from the pure particle-hole shell-model predictions) for a 6^- excitation in ^{40}Ca at the momentum transfer corresponding to the peak of the electron scattering form factor.⁴⁸ This is very similar to the results found in the present analysis for ^{16}O , for instance.

The present analysis treats all known cases of magnetic electron scattering to stretched states in doubly even nuclei, and it spans a wide range of hole states ($l_a = 1, 2, 3, 4, 6$) and particle states ($l_b = 2, 3, 4, 5, 7$). Realistic radial wave functions have been included, and the results of including meson exchange currents have been discussed. For light nuclei, where experimental results are most complete, we conclude that there is no significant quenching of isovector stretched magnetic strength from the simple single-particle sum rules, and invocation of exotic effects does not appear to be appropriate.

ACKNOWLEDGMENTS

We would like to thank M. A. Plum for permission to use his data and for several enlightening conversations, and H. M. Duiker for assistance in the early stages of the calculations. This work was supported in part by the U.S. Department of Energy.

*Present address: Institute of Nuclear and Particle Physics and Physics Department, University of Virginia, Charlottesville, VA 22905.

¹R. A. Lindgren and F. Petrovich, in *Spin Excitations in Nuclei*, edited by F. Petrovich *et al.* (Plenum, New York, 1984), p. 323.

²A. Bohr and B. R. Mottelson, *Phys. Lett.* **100B**, 10 (1981).

³W. Knüpfner, M. Dillig and A. Richter, *Phys. Lett.* **95B**, 349 (1980).

⁴A. Richter, *Nucl. Phys.* **A374**, 177c (1982).

⁵V. R. Pandharipande, C. N. Papanicolas, and J. Wambach, *Phys. Rev. Lett.* **53**, 1133 (1984).

⁶M. Jaminon, C. Mahaux, and H. Ngô, *Nucl. Phys.* **A440**, 228 (1985).

⁷C. N. Papanicolas, in *Nuclear Structure at High Spin, Excitation, and Momentum Transfer (McCormick's Creek State Park, Bloomington, Indiana)*, Proceedings of the Workshop on Nuclear Structure at High Spin, Excitation, and Momentum Transfer, AIP Conf. Proc. No. 142, edited by Hermann Nann (AIP, New York, 1985), p. 110.

⁸I. Hamamoto, J. Lichtenstadt, and G. F. Bertsch, *Phys. Lett.* **93B**, 213 (1980).

⁹A. Amusa and R. D. Lawson, *Phys. Rev. Lett.* **51**, 103 (1983).

¹⁰R. A. Lindgren *et al.*, in *Nuclear Structure at High Spin, Excitation, and Momentum Transfer (McCormick's Creek State Park, Bloomington, Indiana)*, Proceedings of the Workshop on Nuclear Structure at High Spin, Excitation, and Momentum Transfer, AIP Conf. Proc. No. 142, edited by Hermann Nann (AIP, New York, 1985), p. 133.

¹¹R. A. Lindgren *et al.*, *Phys. Rev. Lett.* **47**, 1266 (1981).

- ¹²S. Yen *et al.*, Phys. Lett. **93B**, 250 (1980).
- ¹³DWUCK4, a distorted-wave Born-approximation computer program written by P. D. Kunz, University of Colorado (unpublished).
- ¹⁴C. M. Vincent and H. T. Fortune, Phys. Rev. C **2**, 782 (1970).
- ¹⁵J. S. Dehesa, S. Krewald, A. Lallena, and T. W. Donnelly, Nucl. Phys. **A436**, 573 (1985).
- ¹⁶J. E. Wise, J. S. McCarthy, R. Altemus, B. E. Norum, and R. R. Whitney, Phys. Rev. C **31**, 1699 (1985).
- ¹⁷H. Zarek *et al.*, Phys. Rev. Lett. **38**, 750 (1977).
- ¹⁸F. Petrovich and W. G. Love, Nucl. Phys. **A354**, 499c (1981).
- ¹⁹F. Petrovich, R. H. Howell, C. H. Poppe, S. M. Austin, and G. M. Crawley, Nucl. Phys. **A383**, 355 (1982).
- ²⁰D. B. Holtkamp *et al.*, Phys. Rev. C **31**, 957 (1985).
- ²¹G. G. Simon, Ch. Schmitt, F. Borkowski, and V. H. Walther, Nucl. Phys. **A333**, 381 (1980).
- ²²D. F. Geesaman *et al.*, Phys. Rev. C **30**, 952 (1984).
- ²³M. A. Plum, Ph.D. thesis, University of Massachusetts, 1985.
- ²⁴R. S. Hicks *et al.*, Phys. Rev. C **30**, 1 (1984).
- ²⁵M. A. Plum *et al.*, Phys. Lett. **137B**, 15 (1984).
- ²⁶C. E. Hyde-Wright *et al.*, Phys. Rev. C **35**, 880 (1987).
- ²⁷R. A. Lindgren *et al.*, Phys. Rev. Lett. **46**, 706 (1981).
- ²⁸R. A. Lindgren *et al.*, Phys. Rev. Lett. **40**, 504 (1978).
- ²⁹J. Heisenberg (unpublished).
- ³⁰J. Lichtenstadt *et al.*, Phys. Rev. C **20**, 497 (1979).
- ³¹W. R. Zimmerman, J. J. Kraushaar, M. J. Schneider, and H. Rudolph, Nucl. Phys. **A297**, 263 (1978).
- ³²H. Ikegami *et al.*, Phys. Lett. **74B**, 326 (1978).
- ³³R. O. Nelson, E. G. Bilpuch, C. R. Westerfeldt, and G. E. Mitchell, Phys. Rev. C **30**, 755 (1984).
- ³⁴S. K. Platchkov *et al.*, Phys. Rev. C **25**, 2318 (1982).
- ³⁵T. W. Donnelly and I. Sick, Rev. Mod. Phys. **56**, 461 (1984).
- ³⁶A. E. L. Dieperink and I. Sick, Phys. Lett. **109B**, 1 (1982).
- ³⁷R. J. Peterson *et al.*, Phys. Rev. C **35**, 495 (1987).
- ³⁸R. J. Peterson, H. C. Bhang, J. J. Hamill, and T. G. Master-son, Nucl. Phys. **A425**, 469 (1984).
- ³⁹R. J. Peterson *et al.*, Phys. Rev. C **33**, 31 (1986).
- ⁴⁰C. Ciangaru *et al.*, Phys. Rev. C **29**, 2017 (1984).
- ⁴¹C. Olmer *et al.*, Phys. Rev. Lett. **43**, 612 (1979).
- ⁴²C. Mahaux and R. Sartor, Nucl. Phys. **A468**, 193 (1987).
- ⁴³S. Krewald, A. M. Lallena, and J. S. Dehesa, Nucl. Phys. **A448**, 685 (1986).
- ⁴⁴E. R. Siciliano and D. L. Weiss, Phys. Lett. **93B**, 371 (1981).
- ⁴⁵J. A. Carr *et al.*, Phys. Rev. C **27**, 1636 (1983).
- ⁴⁶R. J. Peterson and J. L. Ullmann, Nucl. Phys. **A435**, 717 (1985).
- ⁴⁷B. L. Clausen, Ph.D. thesis, University of Colorado, 1987.
- ⁴⁸J. Cohen, J. Phys. G **13**, 1497 (1987).